CFD modeling of the transport of human respiratory droplets in an indoor environment

Ole Martinius Harket Norbeck [a,*], Oda Martine Sundsdal [a], Suresh Kumar Nambully [b], Arnab Chaudhuri [a]

[a] *Department of Civil Engineering and Energy Technology, OsloMet – Oslo Metropolitan University, Oslo, Norway*
[b] *Convergent Science GmbH, Linz*
[*] *olenorbeck@hotmail.com*

Abstract

For the last couple of years, the world has faced the global pandemic COVID-19. The viral transmission could occur via different modes like large respiratory droplets, direct contact with contaminated surfaces and airborne microdroplets or aerosol. This work revisits and focuses on human cough, and breathing sequence together with cough in confined spaces. We consider the Eulerian dispersion medium as a multicomponent ideal gas mixture consisting of oxygen, nitrogen and water vapor and the Lagrangian dispersed phase of human cough/breathe is modeled as pure liquid water. The unsteady complex flow is resolved with an advanced three-dimensional multiphase flow solver utilizing adaptive mesh refinement (AMR). A simplified rectangular block with a rectangular mouth area is considered to mimic human beings to inject exhaled gas and liquid droplets associated with cough and or breathing instances. The evaporation model is switched off for the particles of diameter less than 5 μm to resolve the dynamics of the airborne particles. The results clearly demonstrate the efficacy of the novel approach toward gaining more knowledge about viral transmission in indoor environments.

1. Introduction

We are all affected by the ongoing global pandemic, COVID 19 (alternatively called SARS-CoV-2). The serious repercussions following the pandemic have caused communities all over the world to shut down and create a new way of living. The pandemic has highlighted the importance of mitigation procedures concerning the viral spread from humans. Since the beginning of the pandemic, scientists all around the world have shifted their priorities, resulting in a significant surge in research within this field.

Viral transmission takes place in a variety of ways, including inhalation of very fine airborne droplets and aerosols, through droplets and particles depositing on exposed mucous membranes in the mouth, nose, and eyes, and by being in contact with surfaces containing infectious virus. During breathing, talking, singing, coughing, or sneezing, an infected person exhales particles that could be contagious to others. Apart from experimental approaches, Computational fluid dynamics (CFD) has proven to be an effective tool for detailed realistic analysis and eventually plausible design of mitigation measures for indoor environments. One needs to carefully consider several parameters like the local airflow, source proximity, droplet dispersion/evaporation, air change per hour and relative humidity to understand the physics and design such preventive measures. However, resolving the 3D complex flow dynamics of the involved physics is computationally challenging with a high CPU cost. Since the beginning of the pandemic many research articles reported CFD-based analysis of human sneezing [1–3], coughing, breathing, talking [2, 4–12] in various social setups to address the plausible mechanism of viral transmission, social distancing, risk assessments and measures of mitigation. CFD studies in this context mostly used Eulerian-Lagrangian numerical approach to resolve the multiphase flow physics of the governing equations. In a very recent review article [13], an insightful overview of CFD approaches related to respiratory events in buildings towards modeling the airborne and aerosol pathogen transmission is presented highlighting the efficacy of the CFD tool together with the uncertainties and limitations to resolve such complex flow physics. In their study Dbouk and Drikakis [2] and Feng et al. [10] investigated the influence of wind and relative humidity related to human coughs. An increase in droplet sizes can occur due to hygroscopic growth effects which can cause increased deposition fraction on both humans and ground [10]. Gomez et al. [14] mentioned the importance of considering the effects of droplet interactions, especially for the high droplet concentration via scale resolved simulations like large eddy simulation (LES). The studies presented in [15–17] investigated cough instances with LES. Liu et al. [18] performed LES in a restaurant set up highlighting the spatial map of airborne infection risk which revealed the existence of a high aerosol exposure index connected to the reported infection pattern. Burgmann and Janoske [19] presented a study of the transmission of aerosols in a classroom and mentioned the effective application of the air purifier in addition to window ventilation. Both mathematical (Wells–Riley) and numerical (CFD) approaches have been used by Foster and Kinzel [20]. In this regard, Wang et al. [21] also used a coupled CFD and Wells-Riley model to predict the infection probability for passengers on long-distance trains.

The design of ventilation systems is critical to reduce the risk, and many studies [9, 22–24] dealt with the ventilation efficiency, ACH, air filters, and usage of UVC light in different indoor environments. A literature study reported in [25] focused on the existing ventilation strategies of school classrooms. They mentioned that neither natural nor mixing mechanical ventilation are fully capable of dealing with long-range and short-range airborne transmissions, and states that health-based design is required compared to comfort-based design. Their study reported the potential of personalized ventilation systems for the protection of the occupants.

Despite an outpouring of new research articles emerging during the present pandemic, detailed studies of a more realistic combination of human respiratory droplet-producing instances are not abundant. Keeping social distance is challenging in an elevator setup and addressed in studies presented in [5, 6, 9, 11] considering human coughs and breathing events. However, a realistic combination of breathing and cough instances are not considered in these studies. Another important issue is to resolve the smaller respiratory particles (post evaporation) which contribute to forming aerosol particles. For example, Arpino et al. [26] used the Eulerian-Lagrangian model to study non-isothermal aerosol airborne dispersion in a passenger car cabin. They have considered the post-evaporation number and volume distributions in their simulation. Here we attempt to revisit human cough and breathing events in an elevator, considering the Eulerian dispersion medium as a multicomponent ideal gas mixture consisting of O_2, N_2 and H_2O and pure liquid water as the Lagrangian dispersed phase of human cough/breathe. A three-dimensional AMR-based multiphase flow solver (CONVERGE 3.0) [27] is used to resolve the complex unsteady flow dynamics. Some preliminary results using this solver are reported in [28] revealing the effect of relative humidity with fixed air change per hour in an elevator setup for a human cough instance. In this work, we considered a simplified human model and realistic respiratory events of a human cough and breathing sequence in an elevator setup. To resolve the microdroplets after evaporation we set a cutoff particle diameter of 5 μm to switch off evaporation models which effectively mimics the aerosol particles in reality. It is reported in various studies that droplets smaller than approximately 5 μm in diameter can remain airborne for a long time, potentially carrying infectious viruses [29, 30]. The article is organized as follows. In section 2, we present the Eulerian-Lagrangian numerical approach. The computational setup for the different cases is presented in section 3. This is followed by the results and discussion in section 4. Finally, the conclusions are drawn in section 5.

2. Method

The unsteady flow dynamics during instances like breathing, coughing, sneezing, talking or singing in an indoor environment essentially involves fundamental mass, momentum and energy transfer in a multi-component gaseous dispersion medium together with coupled interaction with the dispersed phase arising from aerosol-producing processes. The dispersion medium consisting of oxygen, nitrogen and water vapor, is governed by the 3D compressible Navier-Stokes system of equations together with mass conservation, species conservation, and energy conservation equations. We solve the unsteady Reynolds averaged Navier-Stokes (RANS) formulation and the effects of turbulence are resolved by the Realizable $\kappa - \epsilon$ model. The multi-component dispersion medium is assumed to follow the ideal gas law and the fluid is considered a Newtonian fluid. A Lagrangian approach is adopted for the dispersed liquid phase. The equation of motion is solved for this, considering the drag force and gravity source terms as well as buoyancy and temperature effects. Furthermore, droplet evaporation, droplet collisions, droplet turbulent dispersion, droplet-wall interactions, and droplet breakups are also considered. The detail of the governing equations is not presented here for brevity. We briefly summarize the numerical procedure below.

A three-dimensional finite volume method (FVM) and AMR-based multiphase flow solver (CONVERGE 3.0) is used for this purpose. The predictor-corrector-based Pressure Implicit with the Splitting of Operator (PISO) algorithm is chosen as the solution procedure for the momentum equation and subsequently other transport equations. The solver is based on a collocated finite volume approach together with a Rhie-Chow interpolation scheme to eliminate checker-boarding issues. A 2nd order central scheme is chosen for convective terms which switch to a 1st order upwind scheme with a step limiter to address the non-monotonic behavior for the convective fluxes. On the other hand, the diffusive terms are handled with a 2nd order central scheme. Point-wise successive over-relaxation (SOR) algorithm-based linear solver is used for each governing equation and a first-order implicit Euler scheme is used for time advancement. For the discrete phase, virtual injectors are defined to mimic the droplet-producing instances like breathing and coughing in this work (see figure 2). In accordance with previous studies in the literature, suitable size distributions, injected liquid mass [31, 32] and injection velocity signals are utilized in those instances. For the cough, Rosin-Rammler size distribution, and for breathing, a user-defined log-normal size distribution is employed for the injection of the liquid phase.

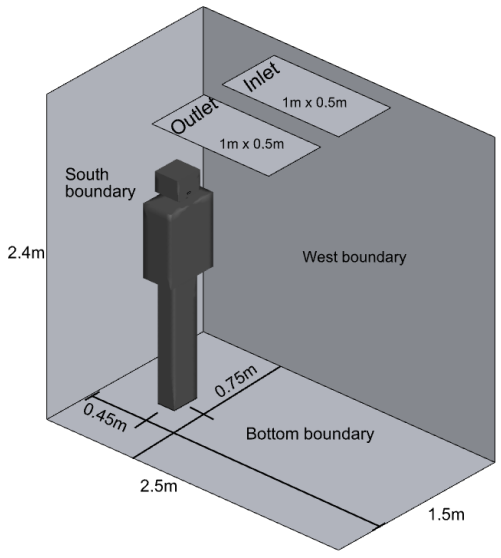

Figure 1: Computational domain of the elevator setup.

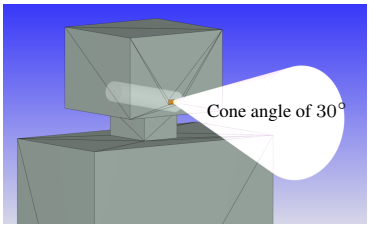

Figure 2: The mouth boundary of the standing human.

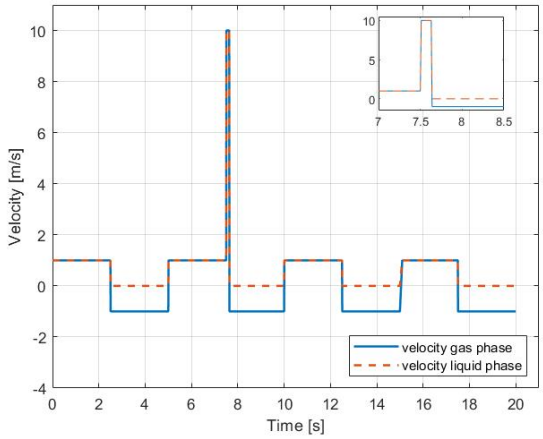

Figure 3: Velocity profiles for breathing signal and cough instance.

3. Problem setup

In this study, we focus on realistic combinations of breathing and cough instances in a confined space. The simulations are performed on a model of an elevator setup (see figure 1), with a base grid of 0.1 m resulting in a cell count of 8911 without embedding or AMR. The air supply and exhaust are placed in the center of the elevator ceiling, each with an area of 0.5 m^2. Air is supplied to the elevator with a supply temperature of 18 $^{\circ}$C and relative humidity of 50 %, which is specified in terms of N_2, O_2 and H_2O, with fractions of 0.760775, 0.231109, and 0.008116 respectively. The airflow rate of the supply air is 270 m^3/h which is equivalent to an air velocity of 0.15 m/s. The simplified model of a standing human is considered with a surface area of 1.9 m^2 and a height of 1.75 m. The mouth is modeled as a rectangle with dimensions of 0.028 m $\times$ 0.0088 m. Figure 2 shows the mouth boundary and the virtual nozzle for the injection of the dispersed phase. The cough and breath are considered as a multiphase mixture consisting of liquid water and air ($O_2 + N_2$) ejected from the mouth through the virtual nozzle, with a specified cone angle of 30 $^{\circ}$ for breathing and 40 $^{\circ}$ for the cough. The turbulence intensity and length scale at the air supply inlet is set to 2 % and 0.003 m respectively, while for the mouth boundary these are assigned as 9.9 % and 0.0011 m respectively. The length scales are 7 % of the hydraulic diameter of corresponding inflow boundaries, as recommended by [33]. The Rosin-Rammler distribution for the cough is assigned with a sauter mean diameter of 73 μm and shape-parameter n=8. On the other hand, the size distribution for breathing particles is based on a log-normal distribution with a mean diameter of 5 μm. The injected droplets are represented by parcels, which is a collection of identical drops with the same properties (same mass, radius etc.), table 1 summarizes the input data for the cough and breathing.

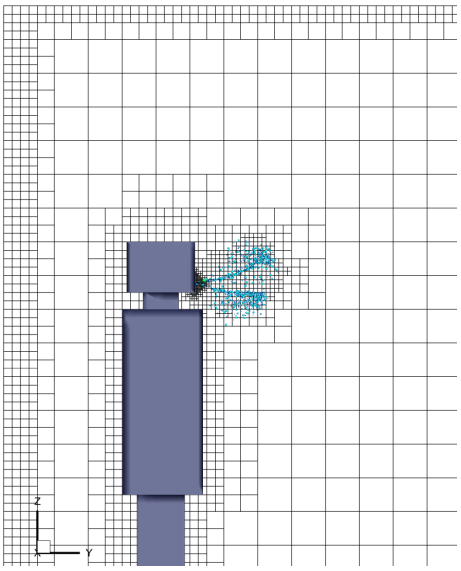

Figure 4: Mesh resolution near the wall boundaries and AMR-based resolution near the mouth at 2 s.

Table 1: Overview of input data

Cough	
Total injected mass	7. 7 mg
Number of parcels	3500
Velocity	10 m/s
Spray cone angle	40 °
Duration of injection	0.12 s
Sauter mean diameter (SMD)	73 μm
Breathing	
Total injected mass	0.033 mg
Number of parcels	1600
Velocity	1 m/s
Spray cone angle	30 °
Duration of injection	2.5 s
Diameter range	0.3-15 μm
Spray model	
Evaporation	Frossling
Collision and coalescence	O'Rourke
Wall interaction	O'Rourke film splash
Droplet breakup	KH-RT
Simulation parameters	
Simulation time	20 s
Initial time step	1-e06 s
Convection CFL limit	1
Diffusion CFL limit	2
Mach CFL limit	500

KH $\equiv$ Kelvin-Helmholtz and RT $\equiv$ Rayleigh- Taylor

We first simulate a single cough instance (Case-1) followed by a realistic breathing (exhale-inhale) sequence embedded with a cough instance (Case-2). Figure 3 illustrates the velocity boundary conditions of the complete signal. Finally, in Case-3, a user-defined function is set to switch off evaporation models when the particle diameter is $< 5\,\mu$m. Simulations are performed till the final physical time reaches 20 seconds for all cases. The flow solver is equipped with AMR functionality which efficiently reduces the computational cost by automatically applying higher mesh resolution in

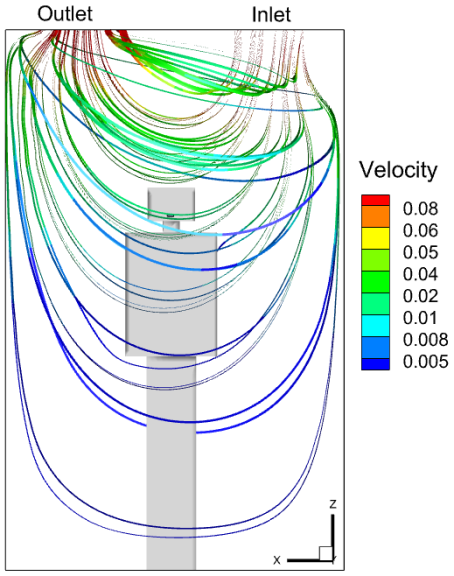

Figure 5: Steady state precursor simulations: streamlines flooded with velocity magnitude.

desired regions where flow-field variations are high while keeping the mesh resolution low elsewhere. The AMR is invoked using a velocity scalar and a passive scalar criteria in CONVERGE. Figure 4 depicts the near wall fixed mesh refinement and AMR-based mesh near the mouth region. For the mouth boundary, we have used an embedding of 10 with a scaling of 5, while for the rest of the boundaries an embedding and scaling of 2 is implemented.

4. Results and Discussions

The transient simulations of the test cases are performed with an initial state of established ventilated space inside the elevator. To achieve this, a precursor steady-state simulation is performed with the desired air supply conditions at the inlet boundary of the computational domain. The simulation is performed until a steady average velocity at the outlet boundary is reached starting from an initially stagnant space. For this steady state simulation, the mouth boundary is considered an impermeable wall. A flow visualisation is presented in figure 5 for this. The wall y^+ values lie in the range of log-layer (not shown) and can be considered sufficient for the two-equation turbulence model equipped with wall functions.

4.1. Single cough

In Case-1, we simulate a single cough instance starting at the beginning. The evolution of the dispersed phase has been illustrated in figure 6. Note that the droplets of the dispersed phase are colored with droplet radius. In this case, we allowed droplets to evaporate completely. It is clear from the colored droplets that the heavier droplets are falling at a faster rate. Noticeably, the dynamics of the droplets depend on the RH and existing airflow pattern in the elevator. A reduction in the mean diameter of the distribution of the evaporating and falling droplets is predicted by the solution (see figure 7). The velocity magnitude reduces to ≈0.5 m/s from the cough injection velocity of 10 m/s. From the dynamics of the droplet and wall film accumulation we noticed that it takes ≈11 s for all the droplets to reach the floor. This is consistent with the acceptable ranges of the evaporation-falling curves mentioned by Xie et al. [34]. Experimental data are required for additional validation. However, the solver has been validated by other studies with similar applications [15–17]. The extent of the spread of the droplet particles under 50 % RH is found to be ≈0.5 m far from the mouth location in front of the human being.

4.2. Breathing and cough

Although the solution of Case-1 can be considered as a verification of the solution procedure, a realistic respiratory signal should consider background breathing instances. In Case-2, we introduce this with a signal as shown in figure 3. Note that a background breathing with exhale-inhale of 5 s is set for this. A single cough is set to occur at 7.51 s during the last phase of the second exhale of the breathing sequence. Two different virtual nozzles are assigned to realize this background breathing signal together with the single cough (figure 2). The time evolution of the droplet dynamics is shown in figure 8. Note that the exhaled breathing particles completely evaporate within a very short time. From previous literature, it can be realized that the micro-droplets of diameter less than 5 μm may remain airborne for a significant amount of time and travel a longer distance. To account for this, a user-defined function is implemented to switch off the evaporation for particle diameters below 5 μm. In Case-3, we simulate the same respiratory signal as Case-2 together with this evaporation cutoff. The gas phase velocity distribution is shown in figure 9. Note that the cough jet velocity decreases rapidly from 10 m/s at the mouth to a low range ≈ 1 m/s very close to the mouth region. The dynamics of the dispersed phase clearly reveal the breathing and coughing particles. Note that the droplets are colored by their size. The violet-colored droplets are arising from the breathing sequence while larger particles are associated with the cough instance. At a later stage, (see figure 10) the dispersion of the droplets in the elevator is dramatically different compared to that predicted in Case-1. The liquid particles reach the east, south and bottom walls as well as the human body surface. The smaller droplets (diameter <5 μm) now represent the combination of the original injection as well as arising due to evaporation of the larger droplets during this time. The distribution of the droplets (having a radius larger than 2.5 μm) at different time instants is illustrated in figure 11. This corroborates the time variation of SMD of the droplet distribution. The present simulation strategy effectively resolves the aerosol behavior under the influence of the existing airflow pattern. The smaller particles remain airborne throughout the simulation time of 20 s for Case-3.

Time evolution of some of the important parameters is compared among the three cases in figure 12. It is evident that the injected respiratory particles are in accordance with the input data mentioned in Table 1 for all cases. The decrease in the particles for Case-1 and Case-2 implies the droplet coalescence and complete evaporation. On the other hand, the signature of the background breathing and cough signal in the evolution of droplets for Case-3 can be noticed. This is also reflected in the liquid mass time-evolution. The orange curve (Case-3) remains above the red curve (Case-2). The droplets reaching any impermeable boundary of the computational domain result in film accumulation accounted for by the wall-droplet interaction model. It is clear that, for a single cough, the film accumulation occurs only on the floor. The film accumulation at this bottom boundary is shown in figure

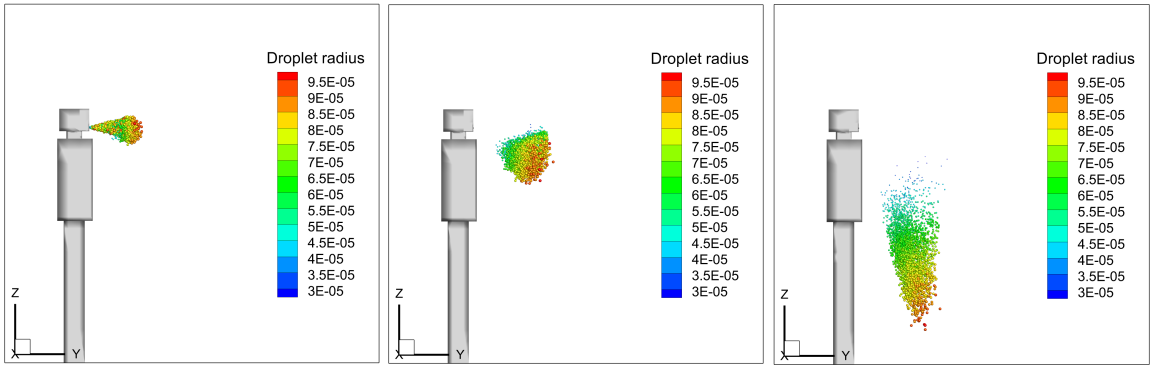

Figure 6: Evolution of dispersed phase for Case-1 at 0.1s, 0.5s and 1.9s.

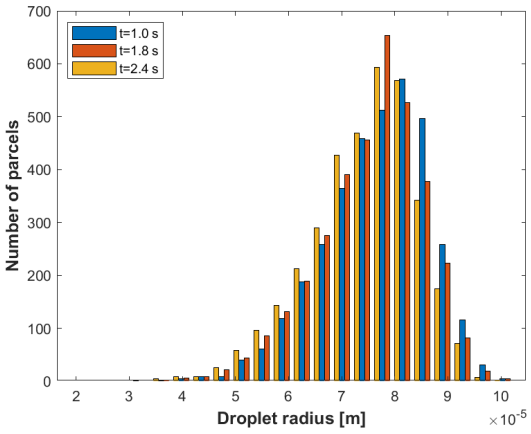

Figure 7: Size distribution for Case-1 at different time instants.

12 for all the cases. A higher film accumulation for Case-2 and Case-3 compared to Case-1 clearly depicts the incorporation of breathing in the respiratory action. Additionally, a marginal film accumulation (not shown) at the south boundary (see figure 1, the wall behind the standing man) is noticed for Case-2. However, for Case-3 due to evaporation cutoff, smaller micro-droplets remain in the domain and film accumulation is noticed in several boundaries (south, east and on the human body surfaces) in addition to the floor. The AMR-based approach to solving transient complex multiphase flow physics is advantageous to achieve lower overall computational costs. We compare the computational cells and total memory usage for Case-2 and Case-3 in figure 13, and it shows that the memory usage increases with time as more particles are injected into the domain. The simulations are performed using 96 processors, resulting in a maximum cost of 144 CPU hours for Case-2, 82 CPU hours for case-3, and less than 10 CPU hours for Case-1. The time-varying cell counts are in accordance with the breathing and cough events. The maximum cell number reaches $\approx$0.158 million when cough action triggers. Evidently, the evolution of the cell counts clearly corroborates the breath-cough signal. The memory usages are found to be in the comparable range among these cases.

We have performed a mesh sensitivity analysis with Case-3. Three different base sizes of the mesh are chosen for this, namely Mesh-1 with 0.2 m, Mesh-2 with 0.1 m and Mesh-3 with 0.05 m. The mesh resolution at the wall boundaries and the mouth boundary are kept consistently similar by varying the embed scale and number of embed layers of CONVERGE setup, and the AMR-based embedding was kept constant as stated before. Figure 14 clearly shows that the results of Mesh-2 and Mesh-3 vary marginally.

5. Conclusions

In this study, we explored a more realistic approach to human cough instances in an elevator setup, where background breathing combined with a cough instance is analyzed. An FVM-based 3D multiphase flow solver equipped with an AMR functionality is used to solve the multi-component compressible dispersion media with the Eulerian approach while the dispersed phase is resolved via the Lagrangian approach. First, a single cough with an active evaporation model is presented to show the capability of the solver to resolve complex transient flow dynamics and evaporation-falling patterns are found to be in accordance with the literature. The respiratory signal consisting of breathing and cough is then studied with the active evaporation model. Since the particles of a diameter less than 5 μm are believed to remain airborne, a user-defined function is implemented to switch off the evaporation to account for this. This implementation makes it clear that the particle dispersion is significantly different from that expected in Case-1, with particles traveling great distances and accumulating on the walls, floor, and human body. Throughout the entire 20 s of the simulation, the particles are still airborne, demonstrating the seriousness of the risk of infection through airborne particles. Results of Case-3 clearly demonstrate the efficacy of the present method to capture the behavior of airborne particles. To the best of our knowledge, a combination of realistic breathing-coughing together with cutoff evaporation to resolve micro-droplets has not been reported in the literature before.

This work forms a basis to gain new knowledge towards understanding airborne viral transmission and designing guidelines for preventive measures in indoor establishments. The future work will involve sensitivity/uncertainty analysis and address the risk assessment in different types of indoor environments with different ventilation strategies utilizing the present method.

Acknowledgment

This work utilized the supercomputing facility of Fram

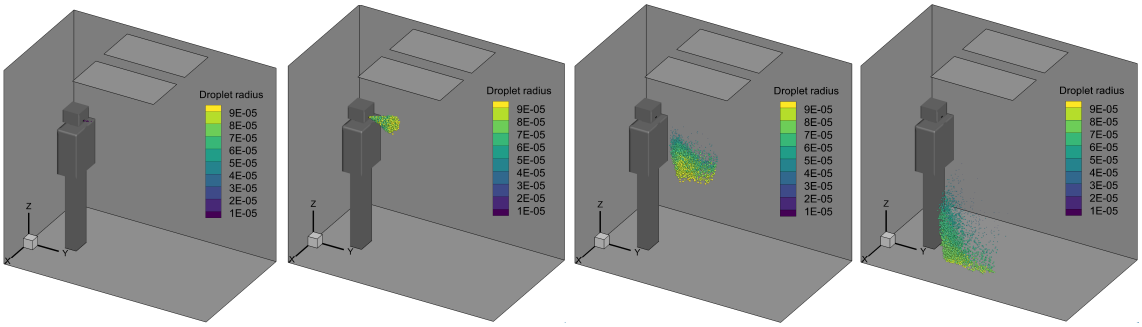

Figure 8: Evolution of dispersed phase for Case-2 at 7.3s, 7.6s, 8.3s and 10.3s.

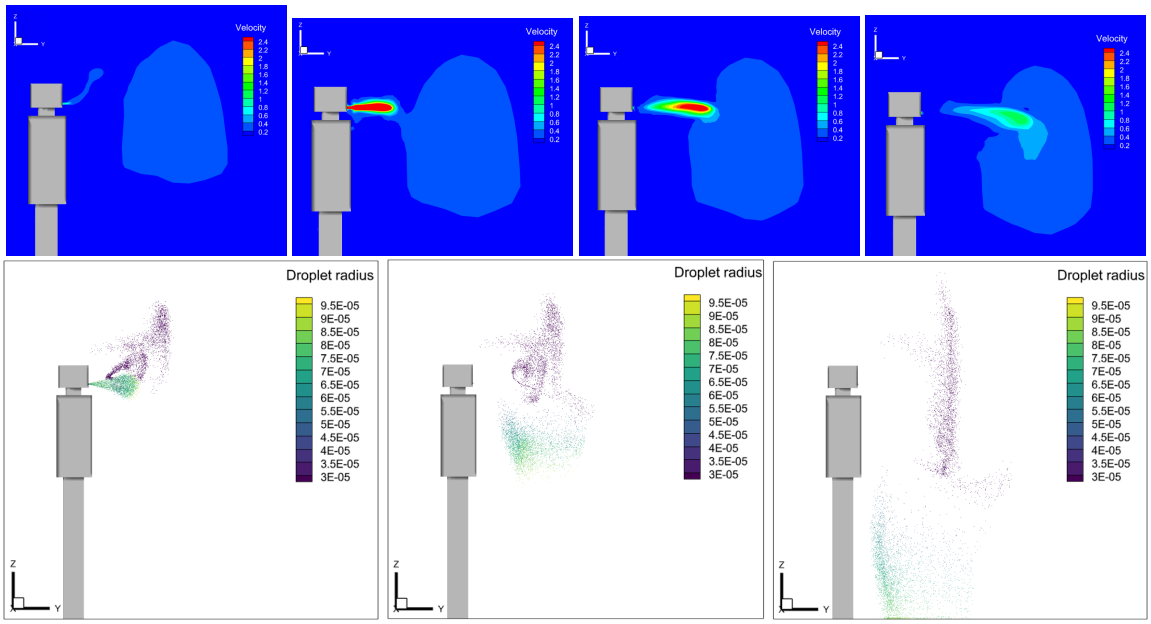

Figure 9: Top row: gas phase velocity contours for Case-3 at 7.0s, 7.6s, 7.7s and 7.9s. Bottom row: evolution of dispersed phase for Case-3 at 7.6s, 8.3s and 10s.

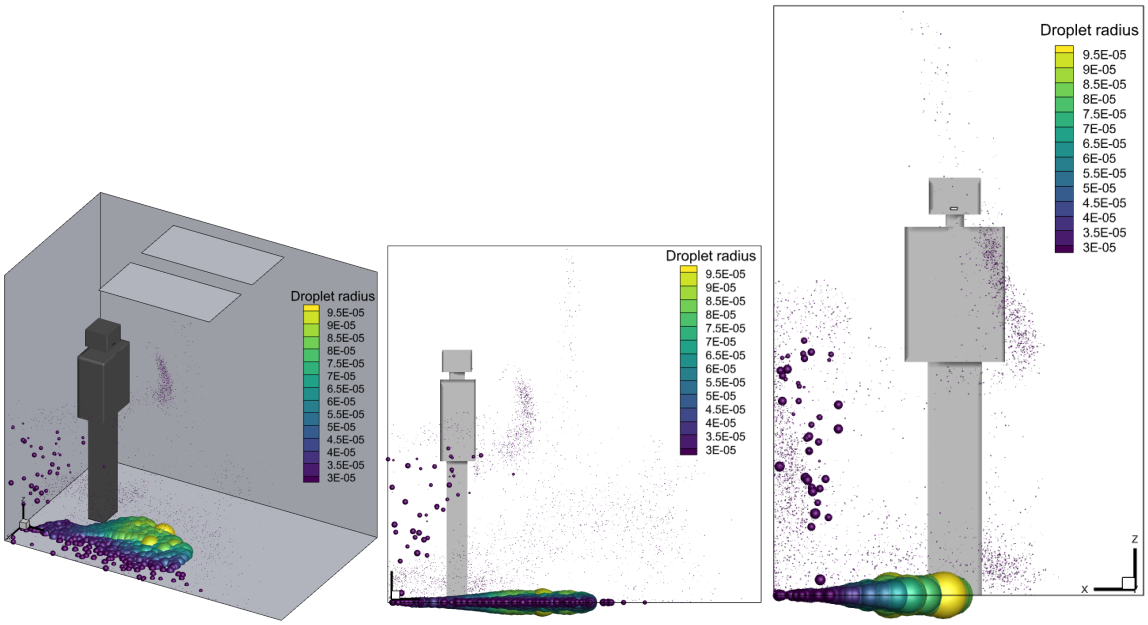

Figure 10: Dispersed phase visualisation for Case-3 at 20s.

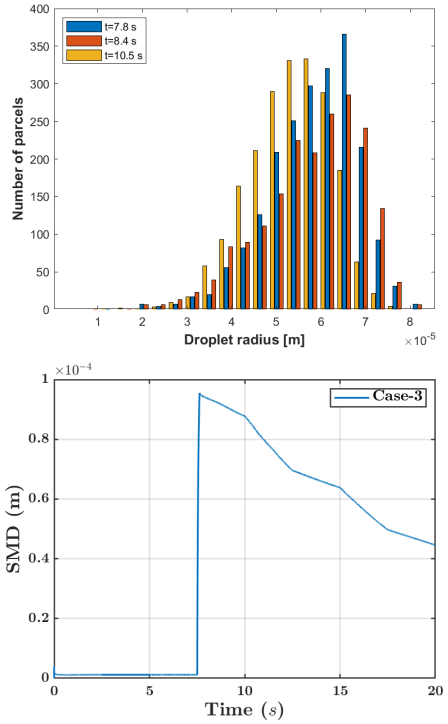

Figure 11: Liquid phase distribution for Case-3 above cutoff size.

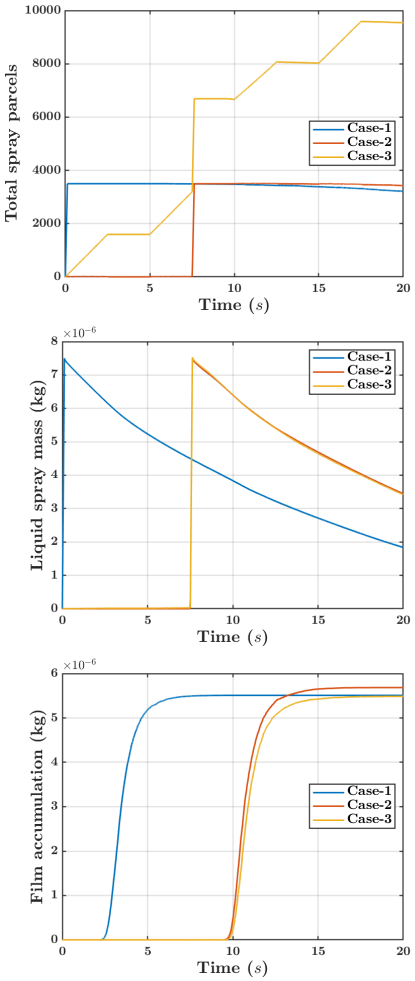

Figure 12: Time evolution of different parameters for three cases.

computer cluster (UiT Arctic University of Norway) under the project NN8005K at Notur, UNINETT Sigma2 AS (National infrastructure for scientific computational science in Norway) as well as local stand alone Windows/Linux machines at OsloMet. The authors of OsloMet greatly acknowledge the collaboration with Dr. Suresh Kumar Nambully of Convergent Science GmbH.

References

[1] G. Busco, S. R. Yang, J. Seo, and Y. A. Hassan, "Sneezing and asymptomatic virus transmission," *Physics of Fluids*, vol. 32, no. 7, p. 073309, 2020.

[2] T. Dbouk and D. Drikakis, "On coughing and airborne droplet transmission to humans," *Physics of Fluids*, vol. 32, no. 5, p. 053310, 2020.

[3] M.-R. Pendar and J. C. Páscoa, "Numerical modeling of the distribution of virus carrying saliva droplets during sneeze and cough," *Physics of Fluids*, vol. 32, no. 8, p. 083305, 2020.

[4] V. D'Alessandro, M. Falone, L. Giammichele, and R. Ricci, "Eulerian–lagrangian modeling of cough droplets irradiated by ultraviolet–c light in relation to sars-cov-2 transmission," *Physics of Fluids*, vol. 33, no. 3, p. 031905, 2021.

[5] N. Sen, "Transmission and evaporation of cough droplets in an elevator: Numerical simulations of some possible scenarios," *Physics of Fluids*, vol. 33, no. 3, p. 033311, 2021.

[6] T. Dbouk and D. Drikakis, "On airborne virus transmission in elevators and confined spaces," *Physics of Fluids*, vol. 33, no. 1, p. 011905, 2021.

[7] Y. Zhou and S. Ji, "Experimental and numerical study on the transport of droplet aerosols generated by occupants in a fever clinic," *Building and Environment*, vol. 187, p. 107402, 2021.

[8] J. K. Gupta, C.-H. Lin, and Q. Chen, "Flow dynamics and characterization of a cough," *Indoor Air*, vol. 19, no. 6, pp. 517–525, 2009.

[9] S. Shao, D. Zhou, R. He, J. Li, S. Zou, K. Mallery, S. Kumar, S. Yang, and J. Hong, "Risk assessment of airborne transmission of covid-19 by asymptomatic individuals under different practical settings," *Journal of Aerosol Science*, vol. 151, p. 105661, 2021.

[10] Y. Feng, T. Marchal, T. Sperry, and H. Yi, "Influence of wind and relative humidity on the social distancing effectiveness to prevent covid-19 airborne transmission: A numerical study," *Journal of Aerosol Science*, vol. 147, p. 105585, 2020.

[11] S. Liu, X. Zhao, S. R. Nichols, M. W. Bonilha, T. Derwinski, J. T. Auxier, and Q. Chen, "Evaluation of airborne particle exposure for riding elevators," *Building and Environment*, vol. 207, p. 108543, 2022.

[12] C. Crowley, B. Murphy, C. McCaul, R. Cahill, and K. P. Nolan, "Airborne particle dispersion by high flow nasal oxygen: An experimental and cfd analysis," *Plos One*, vol. 17, no. 1, p. e0262547, 2022.

[13] Y. Sheikhnejad, R. Aghamolaei, M. Fallahpour, H. Motamedi, M. Moshfeghi, P. A. Mirzaei, and H. Bordbar, "Airborne and aerosol pathogen transmission modeling of respiratory events in buildings: An overview of computational fluid dynamics," *Sustainable Cities and Society*, p. 103704, 2022.

[14] A. Gomez-Flores, G. Hwang, S. Ilyas, and H. Kim, "A cfd study of the transport and fate of airborne droplets in a ventilated office: The role of droplet-droplet interactions," *Front. Environ. Sci. Eng.*, vol. 16, no. 3, pp. 1–14, 2022.

[15] S. Trivedi, S. Gkantonas, L. C. Mesquita, S. Iavarone, P. M. d. Oliveira, and E. Mastorakos, "Estimates of the

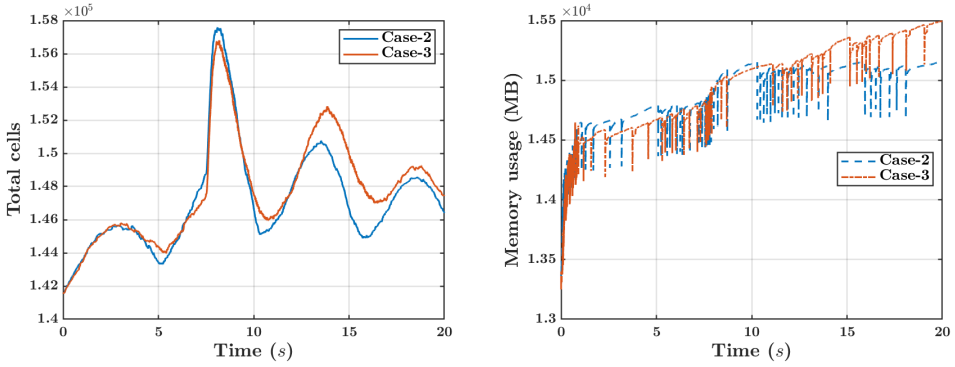

Figure 13: Computational cells and total memory usage for cough and breathing cases.

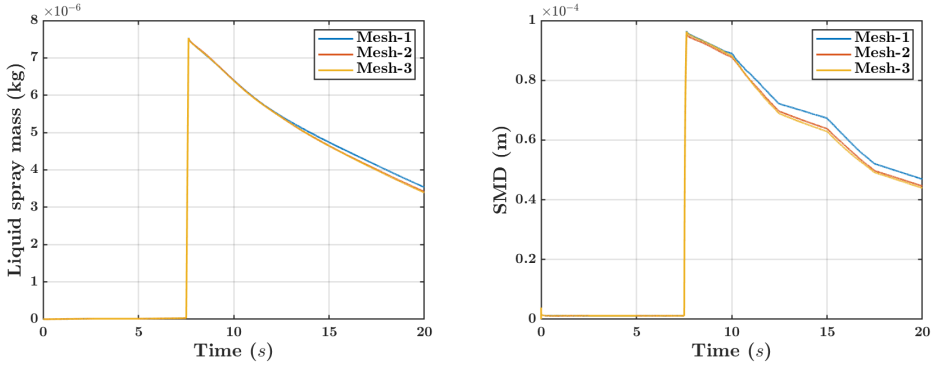

Figure 14: Mesh sensitivity analysis for Case-3.

stochasticity of droplet dispersion by a cough," *Physics of Fluids*, vol. 33, no. 11, p. 115130, 2021.

[16] H. Ge, L. Chen, C. Xu, and X. Cui, "Large-eddy simulation of droplet-laden cough jets with a realistic manikin model," *Indoor and Built Environment*, p. 1420326X211032247, 2021.

[17] H. Ge, P. Zhao, S. Choi, T. Deng, Y. Feng, and X. Cui, "Effects of face shield on an emitter during a cough process: A large-eddy simulation study," *Science of The Total Environment*, vol. 831, p. 154856, 2022.

[18] H. Liu, S. He, L. Shen, and J. Hong, "Simulation-based study of covid-19 outbreak associated with air-conditioning in a restaurant," *Physics of Fluids*, vol. 33, no. 2, p. 023301, 2021.

[19] S. Burgmann and U. Janoske, "Transmission and reduction of aerosols in classrooms using air purifier systems," *Physics of Fluids*, vol. 33, no. 3, p. 033321, 2021.

[20] A. Foster and M. Kinzel, "Estimating covid-19 exposure in a classroom setting: A comparison between mathematical and numerical models," *Physics of Fluids*, vol. 33, no. 2, p. 021904, 2021.

[21] Z. Wang, E. R. Galea, A. Grandison, J. Ewer, and F. Jia, "A coupled computational fluid dynamics and wells-riley model to predict covid-19 infection probability for passengers on long-distance trains," *Safety Science*, vol. 147, p. 105572, 2022.

[22] F. Mohamadi and A. Fazeli, "A review on applications of cfd modeling in covid-19 pandemic," *Arch Computat Methods Eng*, pp. 1–20, 2022.

[23] H. Motamedi, M. Shirzadi, Y. Tominaga, and P. A. Mirzaei, "Cfd modeling of airborne pathogen transmission of covid-19 in confined spaces under different ventilation strategies," *Sustainable Cities and Society*, vol. 76, p. 103397, 2022.

[24] C. Anuraghava, K. Abhiram, V. N. S. Reddy, and H. Rajan, "Cfd modelling of airborne virus diffusion characteristics in a negative pressure room with mixed mode ventilation," *International Journal for Simulation and Multidisciplinary Design Optimization*, vol. 12, p. 1, 2021.

[25] E. Ding, D. Zhang, and P. M. Bluyssen, "Ventilation regimes of school classrooms against airborne transmission of infectious respiratory droplets: A review," *Building and Environment*, vol. 207, p. 108484, 2022.

[26] F. Arpino, G. Cortellessa, G. Grossi, and H. Nagano, "A eulerian-lagrangian approach for the non-isothermal and transient cfd analysis of the aerosol airborne dispersion in a car cabin," *Building and Environment*, vol. 209, p. 108648, 2022.

[27] K. Richards, P. Senecal, and E. Pomraning, "Convergent science, converge 3.0*." https://convergecfd.com/.

[28] P. Patrick, "Analysis of human cough in confined spaces: a numerical study," master's thesis, Institutt for bygg- og energiteknikk, Oslo Metropolitan University, 2021.

[29] S. Asadi, N. Bouvier, A. S. Wexler, and W. D. Ristenpart, "The coronavirus pandemic and aerosols: Does covid-19 transmit via expiratory particles?," 2020.

[30] K. A. Prather, C. C. Wang, and R. T. Schooley, "Reducing transmission of sars-cov-2," *Science*, vol. 368, no. 6498, pp. 1422–1424, 2020.

[31] T. Dbouk and D. Drikakis, "On respiratory droplets and face masks," *Physics of Fluids*, vol. 32, no. 6, p. 063303, 2020b.

[32] X. Xie, Y. Li, H. Sun, and L. Liu, "Exhaled droplets due to talking and coughing," *Journal of the Royal Society Interface*, vol. 6, no. suppl_6, pp. S703–S714, 2009.

[33] H. K. Versteeg and W. Malalasekera, *An introduction to computational fluid dynamics: the finite volume method*. Pearson Education Limited, 2. edition ed., 2007.

[34] X. Xie, Y. Li, A. Chwang, P. Ho, and W. Seto, "How far droplets can move in indoor environments–revisiting the wells evaporation-falling curve.," *Indoor Air*, vol. 17, no. 3, pp. 211–225, 2007.